

"30 "31 "32 "33 "3B "3C "3D "01 "02 "10 "03 "04 "11 "3E "3F "1D "18 "23 "16 "72  
"73 "74 "75 "76

Dr. Cornelius Gahl

# Advanced Internship of the Bachelor of Physics, WS 24/25

## Versuch Ba10

TutorIn: Bharti Mahendru

Versuchsname : STM - Scanning Tunneling Microscopy

Konstantin Bernhardt, Maria Bentert, Benedict Steil

7th July 2025

---

## Contents

<b>1</b>	<b>Introduction</b>	<b>3</b>
<b>2</b>	<b>Theoretical Basics</b>	<b>3</b>
2.1	Setup and Function of a STM . . . . .	3
2.1.1	Setup - Coarse Approach . . . . .	4
2.1.2	Software Setup - WSxM Software . . . . .	5
2.2	Feedback and Controlling Circuit . . . . .	5
2.2.1	constant hight . . . . .	5
2.2.2	constant current . . . . .	6
2.2.3	Quantum Tunneling . . . . .	6
2.3	Fourier Transformation . . . . .	7
2.4	Piezoelectric effect . . . . .	8
2.5	Graphite . . . . .	8
2.6	Layer Stacking and Graphite Formation . . . . .	9
<b>3</b>	<b>Results</b>	<b>10</b>
3.1	Varying of the Parameters . . . . .	10
3.2	Determination of the Distance between different graphite planes . . . . .	11
3.3	Atomic-Structure and -Symmetry . . . . .	14
<b>4</b>	<b>Fourier transform</b>	<b>19</b>
<b>5</b>	<b>Conclusion</b>	<b>21</b>

# 1 Introduction

In its simplest formulation, the typical use of a Scanning Tunneling Microscope is to examine a surface at an atomic scale. More accurately probing the conductive surface of a sample for its topography and electronic structure. To achieve this, a very sharp and very accurately controlled movable metallic tip is used to obtain a constant tunneling current. The image of the movements of the tip yields the surface topography of the sample, its structure.

In this report scanning tunnel spectroscopy (STM) is used to find different characteristics of highly orientated pyrolytic graphite (HOPG), such as the determination of the lattice constant and the analysis of the atomic lattice for symmetries and angles between atomic directions.

## 2 Theoretical Basics

### 2.1 Setup and Function of a STM

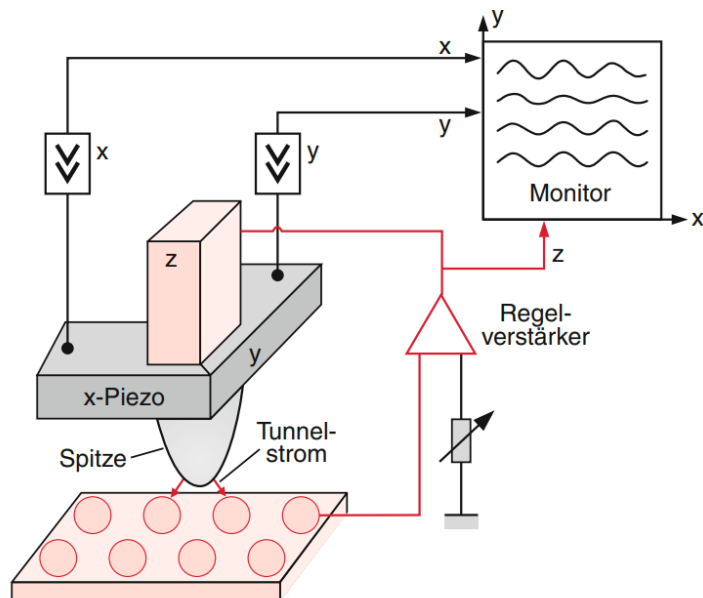


Figure 1: Setup of the STM.[1]

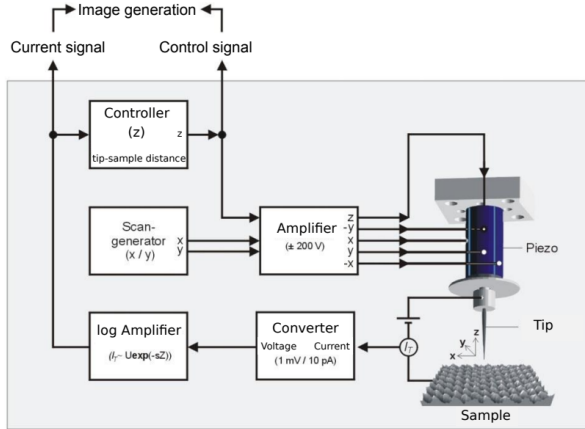


Figure 2: Setup of the STM/STS.[2]

### 2.1.1 Setup - Coarse Approach

The setup of the scanning tunneling microscope (STM) is used to either mainly probe the topography and have the measurement affected by the electronic structure due to the dependence of the tunneling current (2.2.3) or not as STM but STS (scanning tunneling spectroscope) to probe concerning the electronic density of states in the surface of an sample. The first application uses the control signal in (2) and the second application uses the current signal. For the measurements and conclusions in this protocol, a STM was custom-designed for use under atmospheric pressure by AG Franke (FU Berlin) [3]. This STM is operated and visualized through the graphical user interface (GUI) of the Nanotec control system. This system utilizes digital-to-analog converters to drive the X and Y axes of the piezoelectric scanner, while an analog-to-digital converter monitors the Z-axis voltage output from the conversion of the tunneling current (typically  $10^{-12}$  A) into a voltage signal. Interaction between the control hardware and the computer (2.1.2) is established via a PC, using the free WSxM [9] software provided by Nanotec. Also data acquisition and imaging, as for post-processing and analysis are carried out using WSxM. The probe assembly for the STM is primarily composed of a piezoelectric tube scanner with a 90% Platinum and 10% Iridium tip, which is first manually brought close to the sample using a precision micrometer screw and a camera (optic microscope). Such that there is only a small gap in between the tip and its reflection, seen on the camera image. The further approach is performed by a computer-controlled step-motor and is continued carefully until the desired tunneling current is detected. To minimize the influence of external mechanical noise, the entire microscope is positioned on a vibration isolation table and consists of an acoustic isolation cover. This setup ensures stable tunneling conditions.

As outlined the STM system includes several critical hardware components. The piezoelectric tube scanner provides precise control of the position of the tip in all three spatial directions (X, Y, Z) by responding to voltage-induced deformation, enabling sub-Angström ( $\text{\AA}$ ) resolution. A high-voltage amplifier (up to  $\pm 200$  V) converts control signals into drive voltages for the scanner. The scan generator defines the lateral (X/Y) raster movement across the sample surface. To maintain a constant tunneling current, a feedback controller adjusts the Z-position dynamically based on input from the current-to-voltage (analog-to-digital) converter. A logarithmic converter is also included (but optional) to linearize the inherently exponential dependence (2.1.2) of the tunneling current of the tip-sample-distance ( $d$ ), for a more stable (i.e. no large jumps) signal and therefore better analysis. Together, these components enable accurate tip positioning, signal detection, and feedback regulation, as this will become clearer in the following.

### 2.1.2 Software Setup - WSxM Software

After the initial setup (the coarse approach) is completed, the stepper motor system is mounted, and the Approach menu is accessed via the software interface. The automated fine approach is initiated by selecting the Fine Approach function. During this process, the system gradually lowers the tip toward the surface until a measurable tunneling current is detected. Once the status message in range appears, the approach procedure is considered complete. At this point, the Approach window is closed, and the Secure function is activated to maintain the position of the tip. Subsequently, the stepper motor is removed, the camera is switched off, and the acoustic isolation cover is placed over the STM. Scanning is initiated by deactivating the Secure mode. The feedback electronics then automatically adjust the tip-sample-distance to reach the predefined tunneling current (referred to as the Setpoint current). Once this condition is met, scan image acquisition begins and is displayed in real time. Scanning parameters (3) such as image size and resolution can be modified during active tunneling in order to optimize coverage and image quality. If the scanning process needs to be paused or interrupted, the Secure function is reactivated, which causes the tip to retract safely from the surface. The scan image is continuously updated on screen. To save a captured scan, the floppy disk icon is selected. The file is then stored in a predefined directory. These images can subsequently be processed and visualized through the Representation menu of the software. Before replacing the tip, it is manually retracted entirely from the sample. All offset values in X, Y, and Z are reset to zero, the bias voltage is set to  $10^3$  mV, and the Z-gain is adjusted to 10. The measurement session is concluded by selecting the Stop button. This shutdown procedure is followed prior to any tip or sample exchange to prevent mechanical damage or electrical discharge.

STM menu			
Parameter	Description	Manual approach	Imaging
Size (nm)	Size of the square scanning area	[0 nm	1 - 50 nm]
Speed (lines/sec)	Scan speed	2	$\propto$ 4 to 1
Points	data points per line	256	256
X / Y off (nm)	offsets of scan area	0	...
Z off (nm)	offset of zero point along Z	adopt!	
Angle	Rotation of image	0	0
Bias (mV)	voltage applied to sample	+ 1000 mV	$\pm$ 30 - 1000 mV
Set point	tunneling current	1 nA	1 nA - 30 nA
Signal Gain	amplification factor	1	1
Z Gain	HV amplification for Z scan (10 - max.)	10/5/3/1	
XY Gain	HV amplification for X,Y scan		
P	proportional gain	0.12 - 0.06	
I	integral gain	P/2: 0.06 - 0.03	

Figure 3: Parameters of WSxM control software.[3]

## 2.2 Feedback and Controlling Circuit

Using the piezoelectric crystal, the tip is now moved across the sample to obtain topographical information about the sample. There are two basic methods for obtaining the height of the sample at a specific location (x, y):

### 2.2.1 constant hight

Using this method the tip is getting moved across the sample maintaining a constant hight. Through measuring the tunneling current, the actual hight of the sample is being acquired. One benefit of this method is its speed. Although, when having an uneven sample, the tunneling current may vary highly, which might lead to high errors. If the settins are not chosen carefully, the tip might even come into contact with the sample.

### 2.2.2 constant current

Here, the height of the tip is adjusted via a control loop so that the measured tunneling current at every point equals a preset current, thus keeping the tunneling current constant. The sample map is then created directly from the three-dimensional positions of the tip. By continuously adjusting the height of the tip, this method can also measure samples with rough surfaces and larger atomic protrusions. However, this process is slowed down by the control loop compared to the constant height method.

In the control loop, the measured tunneling current (controlled variable) is compared with the target tunneling current (reference variable). The difference between the two is used to calculate the voltage required at the z-piezo (manipulated variable) to change the height of the tip so that the desired tunneling current is measured.

The parameters proportional and integral gain are to significant importance in the control loop. The proportional gain acts like an instant reaction to current changes. The tip height gets corrected by comparing the measured tunneling current and target tunneling current.

The integral gain on the other hand corrects accumulated error over time.

### 2.2.3 Quantum Tunneling

Any current is made by moving charges in a certain interval in time.

$$I = \frac{dQ}{dt} \quad (1)$$

A potential barrier (4) set by a vacuum separates the electrons in binding states of the sample surface and those in binding states of the tip, i.e. the electrons can not move from the states of one side to the ones on the other. Because the tip and the surface are connected via the closed circuit (without voltage), the Fermi levels are equal and therefore the electrons would not move through the vacuum if they could. Then there is a voltage (Bias=V) put on the tip and the surface. One is on mass ( $V_t = 0 \Rightarrow E_t = E_{t_0} + 0$  (potential and energy of the tip and it's levels)) and for the other the energy levels are changed by  $V_s = V(3)$ , and therefore  $E_s = E_{s_0} + eV$  (potential and energy of the sample and it's levels). That concludes in unoccupied states in the sample higher than  $E_{F_{s_0}}$  (Fermi levels before bias) and a now sloping potential barrier. Therefore these states can be occupied by the electrons of the tip and they are with a certain probability  $T[8]$ :

$$\kappa = \frac{\sqrt{2m(\Phi_{eff} - E)}}{\hbar} \quad (2)$$

$$T \propto e^{-2\kappa d} \quad (3)$$

Which is correlated with the descent of the probability for electrons to be located further away from both the tip and the sample [8]

$$\psi = \psi_0 e^{-\kappa z} \quad (4)$$

Such that the probability to find any certain electron with certain energy  $E$  on the surface  $z = 0$   $\psi_0$  descends proportional to  $(T^{\frac{1}{2}})$ , where  $z$  equals the distance from the tip. This means to get sample and tip close enough together, means to get a possibility for electrons to tunnel through the gap  $T \neq 0$  and to get  $\psi_t$  overlap with  $\psi_s$ . Of course it is important how many states there are (density of states  $\rho_{s,t}(E)$ ) to be changed by the bias voltage and then with what probability those existing states even can be occupied (Fermi-distribution=  $f_E$ ) and how far we are from getting classically over the potential barrier (Work function=Work needed to get the observed electron over the barrier=  $\Phi_{s,t}$ ). For latter, we can use the mean of both work functions  $\Phi_{eff} = \frac{\Phi_s + \Phi_t}{2} + \frac{eV}{2}$  [8], no matter in which direction the bias delays them. The whole dependence of the tunneling current  $I_T$  then looks like this[8]:

$$I_T \propto \int_{-\infty}^{\infty} \rho_t(E) \rho_s(E + eV) T[f(E + eV) - f(E)] dE \quad (5)$$

Now for the setup in use as a STM, wanted is only dependence of the tunneling current on the distance  $d$ :

$$I_T \propto \int_0^{eV} e^{-\kappa d} dE \quad (6)$$

To justify such, we can approximate the Fermi-distribution as rectangular function for the observed energy interval of  $[0, eV]$ <sup>[8]</sup>. Condition being temperature and voltage (bias) so:

$$k_B T \ll |eV| \quad (7)$$

For  $\Phi_{eff}$  and  $\rho_{s,t}$  to be constant in sufficient approximation, the sample and tip are mostly assumed to be homogeneous due to effort in preparation of both, and therefore sufficient is:

$$I_T \propto e^{-\kappa d} \quad (8)$$

Indeed if the tunneling current changes due to changes in the electronic structure ( $\rho_{s,t}$ ) or the work function, these are compensated by adaptation in  $d$ . This yields errors and inhomogeneities in the measurement and the concluding image, which mostly are negligible.

All of these acts are completely analogous for bias and therefore tunneling current, in the other direction, with just every direction-dependent property exchanged between the sample and tip.

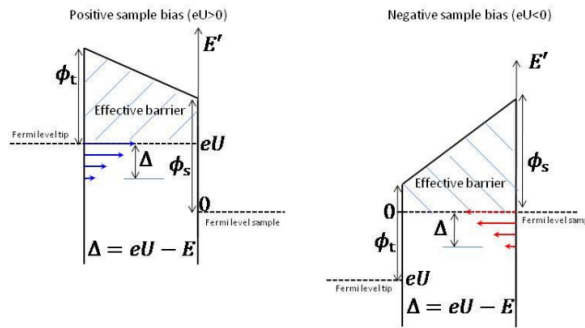


Figure 4: Potential Barriers of current  $U=V$  from tip to sample and the other way around.<sup>[8]</sup>

### 2.3 Fourier Transformation

The Fourier transformation derives from Fourier series, which allow periodic functions to be represented as a combination of sine and cosine functions:

$$f(x) = \frac{a_0}{2} + \sum_{k=0}^{\infty} (a_k \cos(kx) + b_k \sin(kx)) \quad (9)$$

where the Fourier coefficients are:

$$a_k = \frac{1}{\pi} \int_{-\pi}^{\pi} f(x) \cos(kx) dx \quad (10)$$

$$b_k = \frac{1}{\pi} \int_{-\pi}^{\pi} f(x) \sin(kx) dx \quad (11)$$

The  $\sin(kx)$  and  $\cos(kx)$  functions form a set of orthonormal functions. The Fourier transformation extends this concept to aperiodic signals and structures (e.g., transforming lattice structures from real space to reciprocal space). All information of the transformed function is preserved, allowing inverse transformation. The symmetric form of the Fourier transform (in one dimension) is given by:

$$\tilde{f}(k) = \frac{1}{\sqrt{2\pi}} \int_{-\infty}^{\infty} f(x) e^{-2\pi i k x} dx \quad (12)$$

## 2.4 Piezoelectric effect

The piezoelectric effect describes the voltage that occurs when solids are deformed. If a suitable material, a piezoelectric material, is subjected to a corresponding force, the unit cell deforms. This spatial distortion also shifts the center of charge, creating a dipole. Many of these microscopic dipoles act as macroscopic voltage. The inverse of the piezoelectric effect will be much more important for the design of the scanning tunneling microscope. Here, a solid deforms due to the externally applied voltage. The dielectric displacement  $D$  can be described as follows when mechanical stress is applied and an electric field is applied:

$$\mathbf{D} = \epsilon_0 \chi^\sigma \mathbf{E}_{\text{ext}} + \mathbf{P} + \mathbf{d} \cdot \boldsymbol{\sigma} = \epsilon_0 \epsilon^\sigma \mathbf{E}_{\text{ext}} + \mathbf{d} \cdot \boldsymbol{\sigma} \quad (13)$$

Where  $\epsilon^\sigma$  and  $\chi^\sigma$  represent the dielectric and electrical susceptibility tensors, respectively.  $\sigma$  is a constant mechanical stress acting on the crystal, and  $d$  is the piezoelectricity tensor. For the inverse piezoelectric effect, the following equation describes the expansion  $e$  of the crystal:

$$\mathbf{e} = C^E \cdot \boldsymbol{\sigma} + d^t \cdot \mathbf{E}_{\text{ext}} \quad (14)$$

Here,  $C^E$  describes the elastic modulus at a constant electric field and  $d^t$  is the inverse piezoelectric tensor.

## 2.5 Graphite

As the principal quantum number, often denoted as  $n$ , describes the energy level and the average distance of an electron from the nucleus, only one principal quantum number can be partially occupied in a stable state of an atom, with all lower principal quantum numbers being fully occupied. Carbon has six electrons, so the principal quantum number 1 is fully occupied by two electrons and the principal quantum number 2 is occupied by four electrons. In an isolated carbon atom, the 2s orbital is occupied by two electrons (also for energetic reason), and two of the three 2p orbitals each contain one electron (by Hund's rule). However, in bonds with other atoms (including other carbon atoms), it is energetically more favorable for the 2s orbital to combine with one or more 2p orbitals to form so-called hybrid orbitals, where all four orbitals of the second principal quantum number each contain one electron. The following figure shows the three possible hybridizations of the 2s orbital.

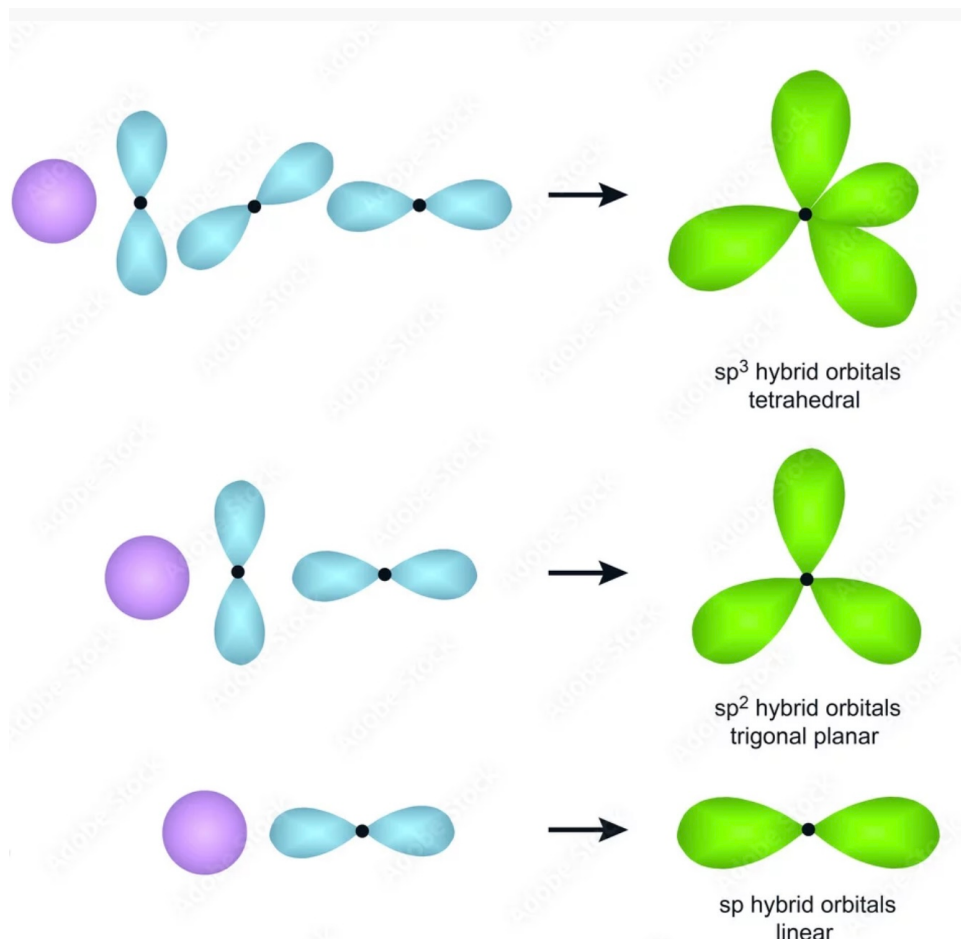


Figure 5: The three possible hybridizations of 2s and 2p orbitals

In case of graphite, the carbon atoms form  $sp^2$  orbitals. The three  $sp^2$  orbitals lie in a single plane, perpendicular to the remaining p orbital, and are separated by an angle of  $120^\circ$ . Due to the  $120^\circ$  bond angles of  $sp^2$  hybridization, carbon atoms can form a two-dimensional hexagonal lattice, called graphene, by repeatedly overlapping their  $sp^2$  orbitals with those of neighboring atoms. This allows for the creation of extensive graphene sheets. Since all angles are equal to  $120^\circ$ , the smallest distance  $d$  between two neighboring atoms is sufficient to characterize the hexagonal lattice.

The covalent bonds within a graphene layer, formed by the overlap of  $sp^2$  orbitals, are exceptionally strong. These strong bonds give graphene remarkable mechanical strength. Additionally, the remaining unhybridized p orbitals, perpendicular to the graphene plane, overlap to form a delocalized electron cloud ( $\pi$  ( $\pi$ ) bonds) across the entire layer. This delocalization of electrons is crucial for graphene's high electrical conductivity within the plane.

## 2.6 Layer Stacking and Graphite Formation

Graphene layers are stacked to form the three-dimensional lattice of graphite. An additional characteristic parameter for graphite is therefore the interlayer distance  $\Delta h$ . The bonding forces between these layers are comparatively weak Van der Waals forces, which allow the layers to slide easily against each other. The energetically most favorable stacking arrangement of these layers is the ABAB stacking (also known as hexagonal close-packed (HCP) stacking), where alternating layers are shifted relative to one another, rather than atoms being directly aligned. This specific arrangement optimizes the weak Van

der Waals interactions. Due to these weak interlayer forces, natural graphite often exhibits significant deviations from ideal stacking. However, highly oriented pyrolytic graphite (HOPG), consisting of well-aligned graphite crystals, can be produced artificially through pyrolysis, a thermochemical process that decomposes organic materials at high temperatures in the absence of oxygen.

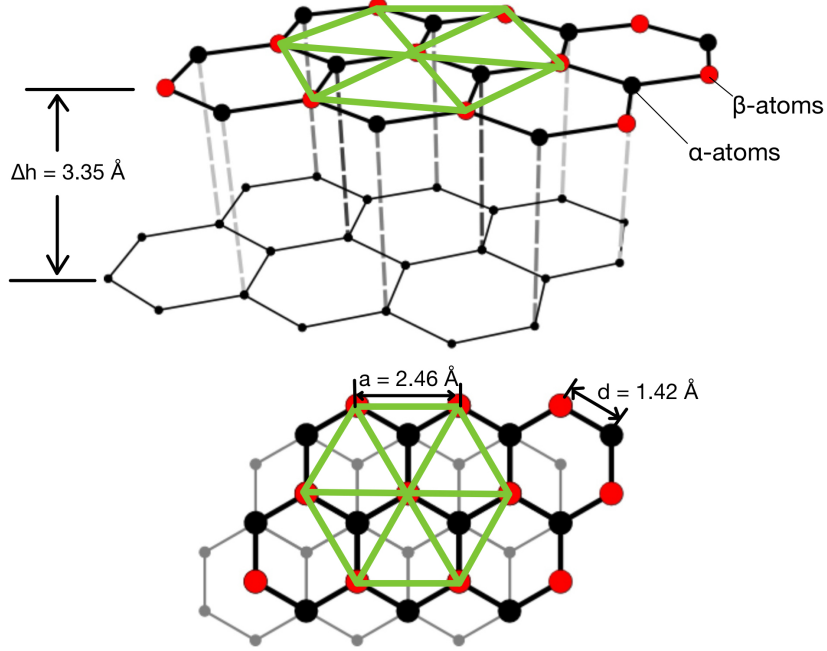


Figure 6: The hexagonal crystal structure of graphite, once viewed from the side and once from the top

In ABAB stacking, half of the atoms in every layer have direct opponents in adjacent layers (these are called  $\alpha$ -atoms), while the other atoms (the  $\beta$ -atoms) have not. The electron distribution in the neighbourhood of  $\alpha$ - and  $\beta$ -atoms is different, so in a surface layer, the  $\alpha$ - and  $\beta$ -atoms seem to have different heights, when viewed by STM. So the STM image of a graphite surface shows a hexagonal lattice of only the  $\beta$ -atoms, i.e. with a lattice constant  $a = \sqrt{3} \cdot d$ .

## 3 Results

### 3.1 Varying of the Parameters

First, a high resolution of the sample was achieved by adjusting the parameters 'Integral gain' and 'Proportional gain', whereby they are coupled and effectively only the 'Proportional gain' can be adjusted. These parameters influence the response of the tip height to changes in the surface, controlled via the control loop. However, these values have no direct physical meaning, because these numbers have no units.

A high 'Integral gain' and 'Proportional gain' causes strong tip reactions on the surface. This can cause the tip to swing open and lead to an incorrect measurement.

In Fig. (7) an image is shown, the lower half of which was taken with the settings P:0.12 and I:0.06 and the upper half with the settings P:1.5 and I:0.75.

It can be clearly seen that the upper half has a poorer resolution. The settings in the lower half were therefore used for the remaining measurements.

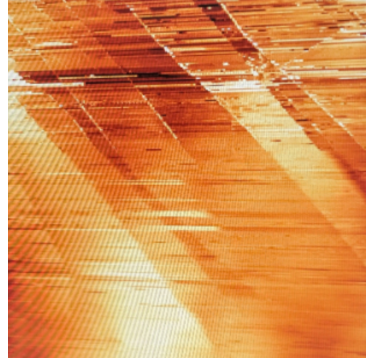


Figure 7: Image of graphite with two different settings, the lower half of which was taken with the settings P:0.12 and I:0.06 and the upper half with the settings P:1.5 and I:0.75.

### 3.2 Determination of the Distance between different graphite planes

With the settings found for clearly visible edges, several images of the graphite surface were now taken (an example is visible in Fig. (8)).

For each Image, it needed to be a new scanning area, to get good statistics.

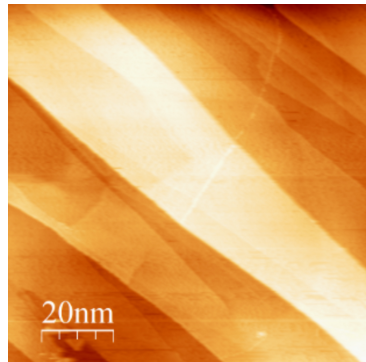


Figure 8: example of graphite with good resolution, which was used to determine the distance between graphite planes

To determine the edge height between two graphite layers, the unfiltered images were opened in the WSxM 5.0 Develop 9.1 software. These images were first processed using the Process-plane-local function to properly orient the image.

In order to do this, the planes, that are supposed to be on one height, are selected. Then the software aligns the whole image according to the Alignment of the selected area.

25 edge heights were measured and plotted according to their size (Fig.(9)). It can be clearly seen that all values between 1nm and 4.5nm are represented in equal frequency, with the literature value of 3.35 nm being four times the error interval of the mean value  $d = (2.81 \pm 0.16)[\text{nm}]$  of the measurement data. It can therefore be assumed that the Z-piezo is poorly calibrated.

A source of error in this setup can be the tip. This tip should only contain one atom so that good resolution is possible. However, this is very difficult to achieve.

Since the tip in our setup was prepared with a pair of sharp scissors, the probability that the tip contained multiple atoms is high. As soon as this is the case, several tunneling currents are measured and an inaccurate result is obtained.

In the following the right calibrations of the z-piezo. In the english wiki instructions of the experiment it says, that in order to measure the correct distance between different graphite planes, the calibration

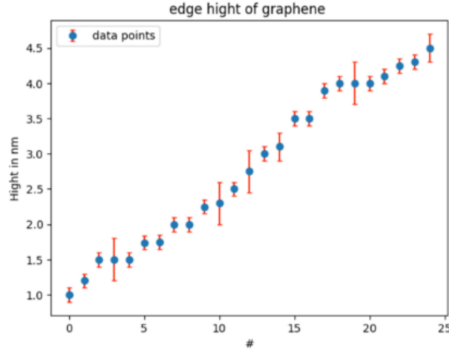


Figure 9: Plot of distance between graphite planes over the Order in hight of these data

should be  $C = 1 \left[ \frac{nm}{V} \right]$ .

In this experiment we could not get any clear value for the distance between different graphite planes, but for the sake of the calculation, we will assume the mean value  $d = (2.81 \pm 0.16)[nm]$  of the measurement data to be our found distance.

The calculation for the correct calibration is now straight forward:

$$C_{correct} = \frac{2.81}{3.35} \cdot C \quad (15)$$

$$C_{correct} = (0.83 \pm 0.48) \left[ \frac{nm}{V} \right] \quad (16)$$

the error of the correct calibration is calculated with Gauss:

$$\Delta C_{correct} = \sqrt{\left( \frac{\partial C}{\partial d} \Delta d \right)^2} \quad (17)$$

$$= \frac{C}{3.35} \cdot \Delta d \quad (18)$$

One good example of one distance between the layers is visible in Fig.(10). The small green line in Fig.(10) is used to read the height profile from the beginning to the end of the line in the graphic. The height profile is shown in Fig.(11).

It can be seen that the jump in the trajectory (the green line in Fig.(11)) represents a distance of  $d = (3.5 \pm 0.2)nm$ , whereby the error was estimated based on the noise in the trajectory to the left and right from the jump.

$$\Delta d = \frac{(Z(4) - Z(6)) + (Z(8) - Z(10))}{2} \quad (19)$$

Where e.g.  $Z(4)$  the value of the green line on the vertical axis in Fig(11) evaluated at  $X = 4$  is.

The calculated distance is within two times the error interval of the literature value. However, as soon as the other values of the measurement data are added, the Fig.(5) follows.

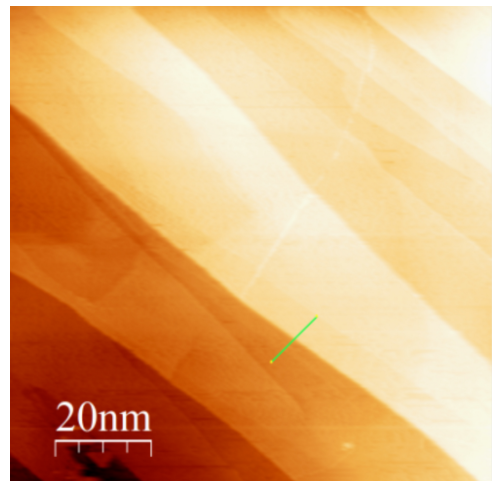


Figure 10: Determination of the hight profile of one edge

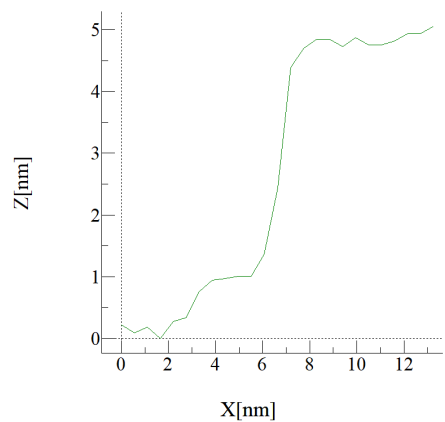


Figure 11: Hight profile of green line in Fig.(6)

### 3.3 Atomic-Structure and -Symmetry

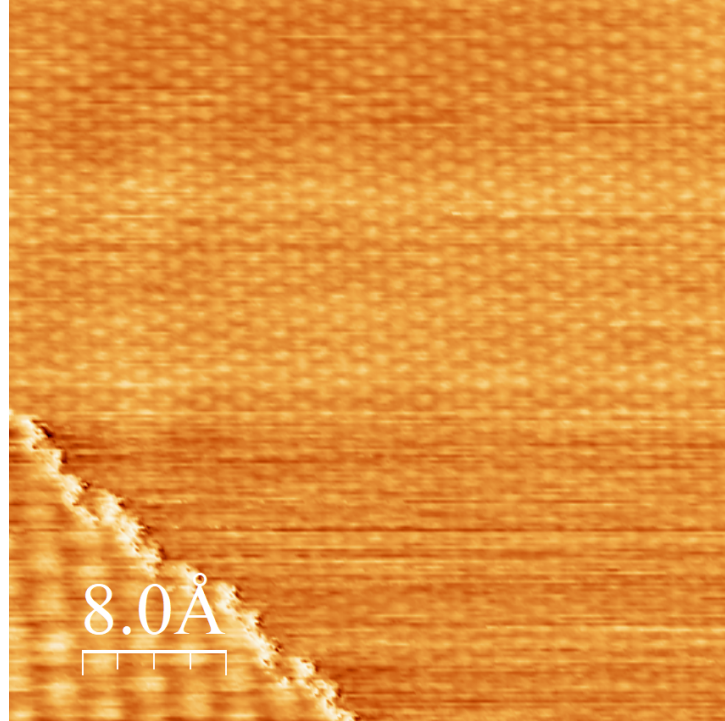


Figure 12: Given Data of the measured atomic structure displayed with WSxM 5.0 [9].

For the analysis of the atomic structure, we attempted to modify the parameters that are set manually. We could not find any set of parameter values that resulted in an image of good and clear resolution. The tutor provided values which are portrayed in (12). Easily seen is the confirmation of the given data representing the theoretically expected structure and symmetry as derived in (2.5). A pattern of periodical level changes, such that the hexagonal atomic structure gets developed. With this, the height from the darker levels to the lighter ones (lower layer to upper layer) is displayed (13) and plotted (14), where for the values two peaks and two minima get focused, by zooming in (15).

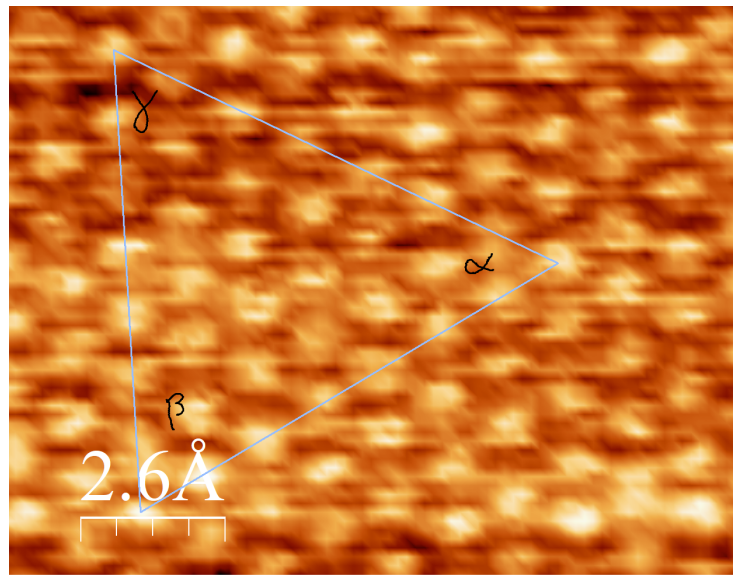


Figure 13: Given Data of the measured atomic structure displayed with WSxM 5.0 [13] zoomed in on (12).

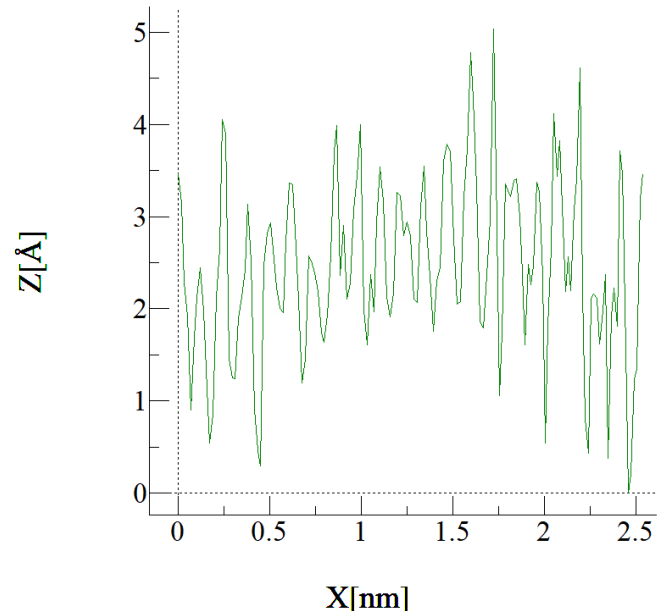


Figure 14: Plot of the height profile across given Data of the measured atomic structure displayed with WSxM 5.0 [9] (13). The distance in  $X$  in nm and the height in  $Z$  in  $\text{\AA}$ .

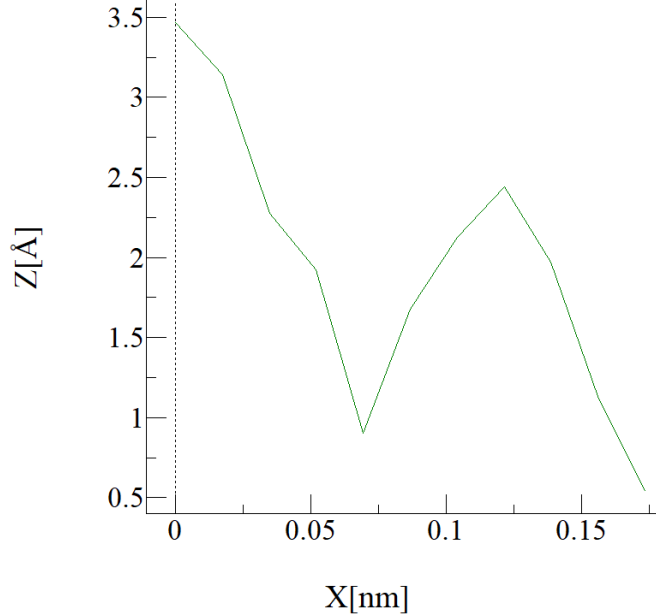


Figure 15: Plot of the height profile across given Data of the measured atomic structure displayed with WSxM 5.0 [9] (14) zoomed in. The distance in  $X$  in nm and the height in  $Z$  in Å.

For the measurement of distance and height to both sides on the connecting straight (13) are the points of measurement are set such that they are in the mean of the peaks or minima (15). The errors are set by half of one scale digit on the  $X$ -axis with

$$\delta X = \pm 0.05 \text{ nm} \quad (20)$$

With Gaussian propagation of errors

$$\delta \Delta X = \delta c = \pm 0.08 \text{ nm} = \pm 0.8 \text{ Å} \quad (21)$$

For

$$\Delta X = |X_2 - X_1| = c \quad (22)$$

$$\delta c = \pm 0.8 \text{ Å} \quad (23)$$

Where  $c$  is the bond length of the sample, the distance in between atoms next to each other in one graphene layer. Chosen for the  $Z$ -axis is also

$$\delta Z = \pm 0.5 \text{ Å} \quad (24)$$

$$\Rightarrow \delta \Delta Z = \delta a = \pm 0.8 \text{ Å} \quad (25)$$

$$\Rightarrow a = \Delta Z = |Z_2 - Z_1| \quad (26)$$

Where  $a$  is half the lattice constant (step height), the distance from the top layer to next one below. The values for  $c$  are taken from the plot (14) starting on the left and going to the right. In (1) the top value for  $c$  is therefore  $\Delta X$  from the peak on the left border (14) to the next to the right. I.e. in the same row are two values for  $\Delta Z = a$ , the top one is taken to the left minimum from the left peak in the plot of those two of which  $c$  is taken in the same row, and the bottom one is  $a$  taken to the right. The errors meet the criteria of half the smallest digit displayed on the scale of (14), but the values are taken on the scale of

(15). That is because the point of measurement, the means of the maxima and minima, are determined by eye. The values of  $c$  are taken with WSxM Representation and Measure of the distances [9]. For  $a$  the determination of values must be done by the markers of WSxM Representation and Measure of the distances, and eye.

Table 1: Measurements from left to right/top to bottom (14) and from top left to top right, to bottom left and to top left again in (13) of  $c$  and  $a$ .

Bond length ( $c$ ) [ $\text{\AA}$ ]	Half Lattice constant ( $a$ ) [ $\text{\AA}$ ]
1.2	- 2.4
1.2	1.5 1.7
1.3	2.8 2.5
1.2	1.9 2.7
1.2	2.4 0.8
1.2	1.3 2.1
1.3	1.3 0.8
1.3	2.1 1.5
1.2	1.5 1.8
1.2	1.5 1.5
1.2	1.2 1.1
1.3	1.4 1.5
1.3	1.8 1.7
1.3	2.7 2.8
1.0	3.1 3.5
1.3	2.0 1.5
1.1	1.0 2.0
1.2	2.5 1.0
1.7	1.5 -
1.7	- -
-	2.5 -

Since the angles between the possible connecting straights are (13)  $\alpha = 57^\circ$ ,  $\beta = 62^\circ$  and  $\gamma = 61^\circ$ , a

mean can be calculated as

$$\theta = \frac{\alpha + \beta + \gamma}{3} = 60^\circ \quad (27)$$

Therefore a hexagonal symmetry or six-fold rotational symmetry, is yielded by a mean angle of

$$\theta = (60 \pm 1)^\circ \quad (28)$$

where the mistake is an educated estimation. For this, expected values are [2]

$$a_l = 3.35 \text{ \AA} \quad (29)$$

$$c_l = 1.42 \text{ \AA} \quad (30)$$

The results as means of the measured values in the table (1) are

$$a_m = (1.8 \pm 0.2) \text{ \AA} \quad (31)$$

$$c_m = (1.3 \pm 0.2) \text{ \AA} \quad (32)$$

$$\delta a_m = \sqrt{\left(\frac{1}{37} \cdot 0.8 \cdot 10^{-10} \text{ m}\right)^2 \cdot 37} \quad (33)$$

$$\delta c_m = \sqrt{\left(\frac{1}{20} \cdot 0.8 \cdot 10^{-10} \text{ m}\right)^2 \cdot 20} \quad (34)$$

Where the mean is just the arithmetic mean over the values in the table and the mistakes are analogue calculated via Gauß. The matching of  $a_l$  and  $a_m$  is possible in 8 times the error interval. The values of  $c_l$  and  $c_m$  match in a simple error interval. This suggests a correct calibration of the X- and Y-Piezo. However, the angles not being exactly the same speaks for some faulty calibration of the X- and Y-Piezos. The very big deviation of the results of the interlayer distance  $a$  from the literature is suggesting especially a very faulty Z-Piezo calibration. In general all factors contributing to the measurement in Z-direction can also contribute to this mistake, and since the used data were not acquired but provided, each of the factors is to be met with an equal amount of consideration towards their responsibility for the deviation. These factors are various systematic and instrumental errors. As touched on before, a key source of error is improper Z-piezo calibration. If the Z-Gain is incorrect, the measured vertical distances deviate systematically from the true step height. Tilted sample mounting introduces geometrical distortion, when the sample surface is not aligned parallel to the XY scan plane, vertical steps appear less due to projection effects. This leads to an underestimation of the step height. Additionally, non-ideal feedback loop settings—particularly poorly tuned proportional and integral gains can impair the ability of the tip to track abrupt and systematic (over longer periods of time) topographical changes. As a result, steps may appear rounded or smeared, obscuring their true vertical extent. Another common issue arises from thermal drift or mechanical vibrations, which can shift the tip or sample during scanning, causing lateral or vertical distortion of the topographic profile, even though the setup is designed not to be influenced by these. Also critical is the tip condition, a contaminated or blunt tip can broaden apparent step edges or introduce multiple contributions by the tip, degrading resolution and introducing ambiguity in step determination. As mentioned, introducing the tunneling current (??), unstable tunneling parameters such as fluctuating bias voltage or tunneling current setpoint can cause a change to the apparent tip-sample distance, leading to inconsistent height measurements.

## 4 Fourier transform

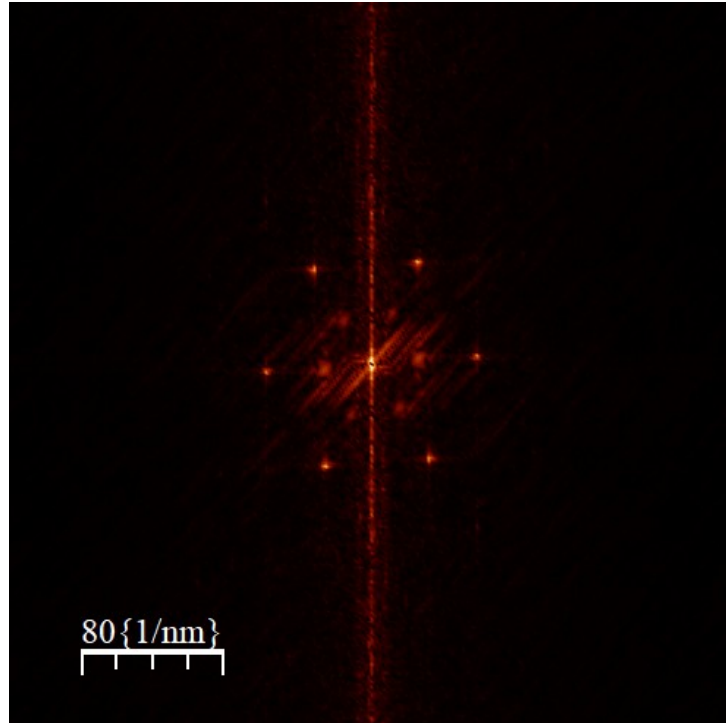


Figure 16: Fourier transform of given data

Using the program WSxM4.0Beta, a Fourier transform of the given data file (fig. 12) was created. The Fourier transform of a hexagonal lattice yields the corresponding reciprocal lattice. The deviations from strict periodicity, which are also visible in the spatial representation, appear in the Fourier transform as additional bright areas that are clearly distinguishable from the lattice points. Therefore, the reciprocal lattice can be measured much more precisely in the FFT image. WSxM4.0Beta was used to draw vectors matching the reciprocal lattice in order to measure the lattice constant. This measurement resulted in three slightly different lattice constants:

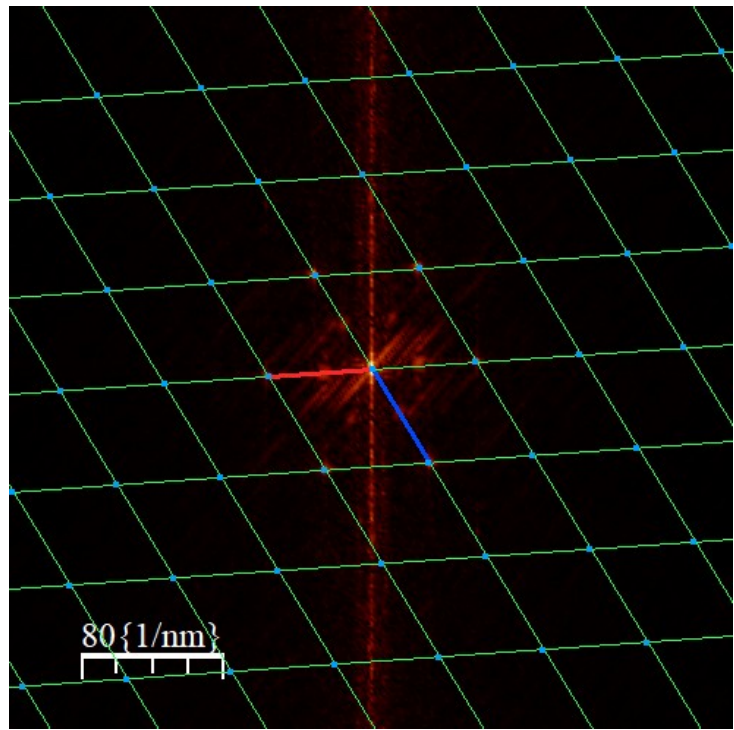


Figure 17: Fourier transform of given data, red vector:  $57.5 \frac{1}{nm}$ , blue vector:  $61.5 \frac{1}{nm}$

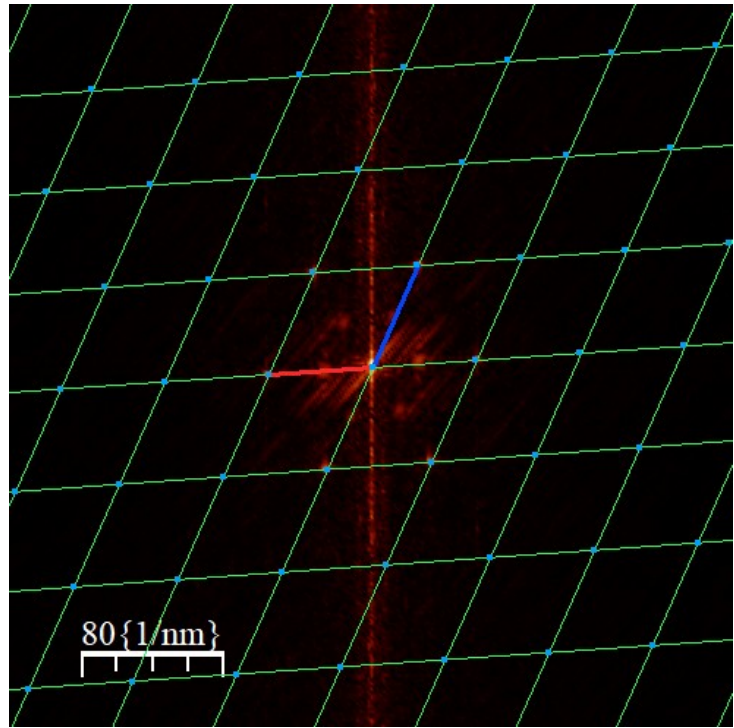


Figure 18: Fourier transform of given data, red vector:  $57.5 \frac{1}{nm}$ , blue vector:  $62.0 \frac{1}{nm}$

The reason could be a different scaling in X- and Y-direction in the original data with a distortion factor of 1.1. This would mean that the measurement in at least one direction is systematically biased, and the

data doesn't allow to determine which axis (i.e. whether the overall results are too small or too large). Therefore we used the minimum and maximum value for further calculation rather than the average value. The relationship between the lattice constant  $a$  in real space and the lattice constant  $g$  of the reciprocal lattice is given by:

$$a = \frac{4\pi}{\sqrt{3}g}$$

Thus, we obtain  $a_{min} = 1.17\text{\AA}$  and  $a_{max} = 1.26\text{\AA}$ . Both values are about half the reference value  $a = 2.46\text{\AA}$  [10]. This is not surprising as fig. 12 obviously doesn't show a hexagonal lattice with a lattice constant of  $2.46\text{\AA}$ . We can only guess about the reason. Again it could be incorrect scaling. But fig. 16 shows an underlying second hexagonal structure that isn't visible in fig. 12. This second lattice has half the lattice constant of the main lattice in fig. 16, yielding in a factor 2 in real space. So if this underlying lattice represented the graphite  $\beta$ -atoms, we would obtain a lattice constant  $a$  between  $2.34\text{\AA}$  and  $2.52\text{\AA}$  with the reference value lying in between. But in this case we actually can't see any reason for a lattice of double density to appear in the data file.

## 5 Conclusion

The found values are not confirming the literature's own. It could not be achieved to get an atomic resolution. There were troubles with the construction, which was the laboratories own, this might have been a major source of these fails to get the results expected. An essential power line was provisionally soldered to the right contact again, after it broke off and the tip was not optimally crafted and the construction was visibly unstable and sensitive to disturbances, as queried by the tutor. The data given by the tutor yielded better results, but because of lack of functionality or knowledge by the evaluator of the program [9], the results did not reach to be a match within one time error interval. this also is influenced by choice of the extent of the interval, which may be, as suggested by these results, chosen to be to small.

A high resolution of the graphite surface was achieved by changing the two parameters 'Integral gain' and 'Proportional gain'. This is well shown in (2.1)

One objective in this experiment was to determine the edge height of two graphite layers. In order to do this multiple Images of the graphite surface were taken. Out of these Images the different edge heights were recorded with the WSxM 5.0 Develop 9.1 software.

It was not possible to get a correct edge height from this data. One of the likely sources of error could be that the tip doesn't just have one atom or the z-piezo was not correctly calibrated.

Also the Calibration of the Z-piezo might not have been correct. So the correct Calibration of  $C_{correct} = (8.29 \pm 0.48) [\frac{nm}{V}]$  was calculated.

The data file provided by the tutor, when displayed with WSxM5.0 (or WSxM4.0Beta), shows a hexagonal lattice, but with a lattice constant of about  $1.2\text{\AA}$  instead of the expected  $2.46\text{\AA}$  [10]. As we were unable to overcome this problem, we performed the required evaluations, but they led to results far away from reference values.

Nevertheless the Fourier transform is a method to evaluate a lattice constant more precisely than by measuring the original STM data. Our Fourier transform showed a distortion in the STM data. We obtained  $a = (1.21 \pm 0.05)\text{\AA}$  or, if there is actually a scaling factor 2,  $a = (2.42 \pm 0.09)\text{\AA}$ .

## References

- [1] Experimentalphysik 3, Wolfgang Demtröder 5.Auflage
- [2] [https://wiki.physik.fu-berlin.de/fp/\\_media/private:ba10\\_anleitung\\_2020-01.pdf](https://wiki.physik.fu-berlin.de/fp/_media/private:ba10_anleitung_2020-01.pdf)
- [3] [https://wiki.physik.fu-berlin.de/fp/\\_media/private:ba10\\_eng2022.pdf](https://wiki.physik.fu-berlin.de/fp/_media/private:ba10_eng2022.pdf)
- [4] <http://www.wsxm.eu/download.html>
- [5] Hugo Strunz, Ernest H. Nickel: Strunz Mineralogical Tables. Chemical-structural Mineral Classification System. 9. Auflage. E. Schweizerbart'sche Verlagsbuchhandlung (Nägele u. Obermiller), Stuttgart 2001, ISBN 3-510-65188-X, S. 51
- [6] [https://stock.adobe.com/de/search?k=s-orbital&asset\\_id=128890949](https://stock.adobe.com/de/search?k=s-orbital&asset_id=128890949)
- [7] <http://u-helmich.de/che/EF/inhaltsfeld-1/9-Kohlenstoff/seite-9-0-2-Modifikationen.html> (edited)
- [8] <https://www.fz-juelich.de/en/pgi/pgi-3/events/lab-courses/18-jara-fit-lab-course-nanoelectronics/jara-fit-lab-course-nanoelectronics-experiments/v17script.pdf>
- [9] <http://www.wsxmsolutions.com>
- [10] [https://wiki.physik.fu-berlin.de/fp/\\_media/private:atamny\\_1999\\_pccp.pdf](https://wiki.physik.fu-berlin.de/fp/_media/private:atamny_1999_pccp.pdf)